LANGMUIR

pubs.acs.org/Langmuir Article

Molecular Mechanism of Ultrasound-Induced Structural Defects in Liposomes: A Nonequilibrium Molecular Dynamics Simulation Study

Viet Hoang Man, Mai Suan Li, Philippe Derreumaux, Junmei Wang, and Phuong H. Nguyen*

Cite This: *Langmuir* 2021, 37, 7945−7954 Read Online

ACCESS | Metrics & More | Article Recommendations

ABSTRACT: The use of ultrasound in combination with liposomes is a promising approach to improve drug delivery. To achieve an optimal drug release rate, it is important to understand how ultrasound induces pathways on the liposome surface where drugs can be released from the liposome. To this end, we carry out large-scale ultrasound-induced molecular dynamics simulations for three single lipid component liposomes formed from the commonly used phospholipids: 1,2-dioleoyl-*sn*-glycero-3-phosphocholine (DOPC), 1,2-dipalmitoylphosphatidylcholine (DPPC), or phosphatidylcholine (POPC). The results show that ultrasound induces the detachment of two leaflets of the DOPC surface, suggesting that the drug release pathway may be through the low lipid packing areas on the stretched surface. In contrast, ultrasound induces pore formation on the surface of DPPC and DOPC, where drugs could escape from the liposomes. While the leaflet detachment and transient pore formation are the mechanisms of DOPC and DPPC, respectively, in both liquid-ordered and liquid-disordered phases, the leaflet detachment mechanism is switched to the transient pore formation mechanism on going from the liquid-ordered phase to the liquid-disordered phase in the POPC liposome. By adding 30% mol cholesterol, the leaflet detachment mechanism is observed in all liposomes. We found that the molecular origin that determines a mechanism is the competition between the intraleaflet and interleaflet interacting energy of lipids. The connection to experimental and theoretical modeling is discussed in some detail.

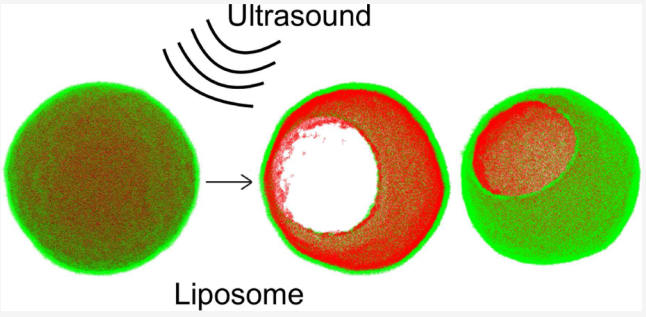

INTRODUCTION

In medicine, an administered drug must penetrate many obstacles in the living system before reaching the desired targets. However, most of the drugs are rapidly cleaned from the blood stream, lacked of targeting and difficult to cross cell membranes, rendering the drug delivery ineffective. Fortunately, these problems have been solved by the use of nanoparticles (NPs), which play a role as drug carriers.[1−5] The basic idea is that NPs carry drugs to desired targets, and then the drugs are released from the NPs by stimuli.[6−13] This way offers several advantages, including improvement of drug stability, bioavailability,[14] highly site-specific delivery,[15] reduced toxicity,[16] and drug release "on demand" without perturbing surrounding cells.

Currently, liposomes are widely used as carriers because of their high biocompatibility and stability.[2,3,17] Ultrasound is an efficient stimulus because it can induce locally and invasively drug release via thermal and/or cavitation effects.[18−22] Therefore, the use of liposomes in combination with ultrasound should provide an excellent method for drug delivery. Understanding the molecular pathways by which ultrasound enhances the permeability of liposomes is therefore of fundamental interest and essential for safe and effective implementation of this method. To this end, various ultrasound experiments have been carried out to measure the rate and identify pathways of released drugs from liposomes.[23−28] Various mathematical and computational models have also been developed to fit and elucidate experimental release rates and pathways.[23,27,29−34] All together, these studies have suggested that ultrasound stimulates drug release through (i) destruction of large parts of the bilayer, (ii) formation of pores on the bilayer, and (iii) diffusion enhanced by the stretched bilayer. However, it is difficult to determine exactly a pathway for a given liposome because it could be affected by various factors such as membrane structure[35] and molecular constituents of the lipid bilayer.[13,23,24,36] Therefore, in this first molecular dynamics (MD) simulation study in the field, we focus on single lipid component liposomes formed by phospholipids widely used in the liposome field: 1,2-dipalmitoylphosphatidylcholine (DPPC), phosphatidylcholine (POPC), and 1,2-dioleoyl-*sn*-glycero-3-phosphocholine (DOPC).[25,27] DPPC is a high

Received: February 25, 2021
Revised: June 3, 2021
Published: June 23, 2021

https://doi.org/10.1021/acs.langmuir.1c00555
Langmuir 2021, 37, 7945−7954

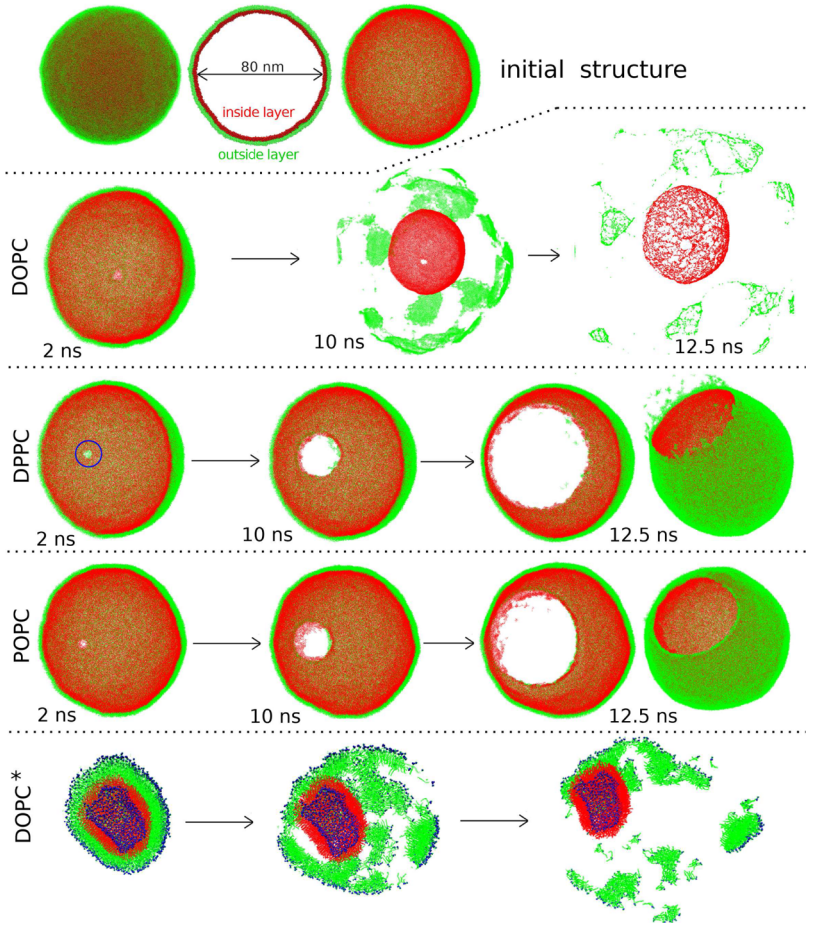

Figure 1. (Top) Initial structure of the DPPC liposome. (Middle) The selected snapshots at various moments of the coarse-grained DOPC, DPPC, and POPC liposomes. (Bottom) The selected snapshots of the all-atom DOPC liposome (denoted as DOPC*). Shown are results obtained from simulations using the ultrasound frequency of 20 MHz and intensity of 640 bar for the DOPC and DOPC* liposomes, 550 bar for the DPPC liposome, and 580 bar for the POPC liposome. For all liposomes, the inner and outer leaflets are colored in red and green, respectively.

melting temperature, ∼41 °C, saturated lipid, while DOPC has a relatively low melting temperature, ∼−17 °C, and unsaturated acyl chains. POPC has one saturated and one unsaturated alkyl chain with melting point at ∼−2 °C. This allows us to investigate the effect of bilayer phase behavior on sensitivity to ultrasound. Experimentally, these liposomes can be well-prepared by different formulation methods;[35] their bilayer phase diagrams were established, and the effects of ultrasound on these phases were also studied.[25,27] In drug-delivery applications, cholesterol (CHL) is usually mixed with lipids to increase the stability of liposomes.[37] Thus, in this study, we also consider three liposomes comprising mixture of CHL with DOPC, DPPC, or POPC with a 70:30 ratio, that is, 70% of lipids and 30% of CHL. All these systems allow us to provide some molecular insights toward the effects of ultrasound and membrane phase behavior on liposome leakage pathways.

METHODS

Construction of Liposomes. In this work, we consider three single-component liposomes, composed of DOPC, DPPC, or POPC lipids, and three DOPC/CHL, DPPC/CHL, and POPC/CHL liposomes, each composed of 70% lipid and 30% CHL. A single-component liposome is constructed by distributing lipids uniformly on the surface of a sphere having a diameter of 80 nm. Given the value of the area per lipid of ∼0.46 nm^2 at 290 K,[38] this results in ∼63,000 lipids for each liposome. For a mixed liposome, we randomly replace 30% of lipids of the single-component liposome by CHL molecules. Each liposome is solvated in a water box consisting of ∼16,331,931 waters. The initial dimensions of the unit cell are $(L_x, L_y, L_z) = (129, 129, 129)$ nm. The coarse-grained MARTINI 2.2 force field[39,40] is employed to describe the membrane and water. We also construct a smaller DOPC liposome with a diameter of 20 nm and use the all-atom CHARMM36 force field[41] together with the TIP3P water model to describe the lipid and water, respectively. As an example, an initial structure of the coarse-grained DPPC liposome is shown in Figure 1. An equilibrium MD simulation is carried out for 500 ns for each system in the NPT ensemble with the pressure P = 1 bar and temperature T = 300 K employing the GROMACS simulation package.[42] The last five structures are used as initial structures for the ultrasound simulations.

Ultrasound MD Simulation. In a conventional simulation, the pressure of the system is maintained at a desired value P_0 by using a barostat, which couples the global pressure of the system to the pressure of the bath by rescaling periodically the lengths of the system[43]

$$\mathbf{r}_i \rightarrow \mu \mathbf{r}_i \qquad (i = 1 \ldots N) \qquad \text{and } L \rightarrow \mu L \tag{1}$$

where N, $\mathbf{r}_i$, and L are, respectively, the number of atoms in the system, the coordinate of the i-th atom, and the length of the system box. The scale factor is given by

$$\mu = \left[1 - \frac{\beta \Delta t}{\tau_P}(P(t) - P_0)\right]^{1/3} \tag{2}$$

where Δt, $P(t)$, β, and τ_p are the integration time step, the instantaneous pressure in the system, the isothermal compressibility, and the temperature coupling constant, respectively. The lengths of the system

https://doi.org/10.1021/acs.langmuir.1c00555
Langmuir 2021, 37, 7945−7954

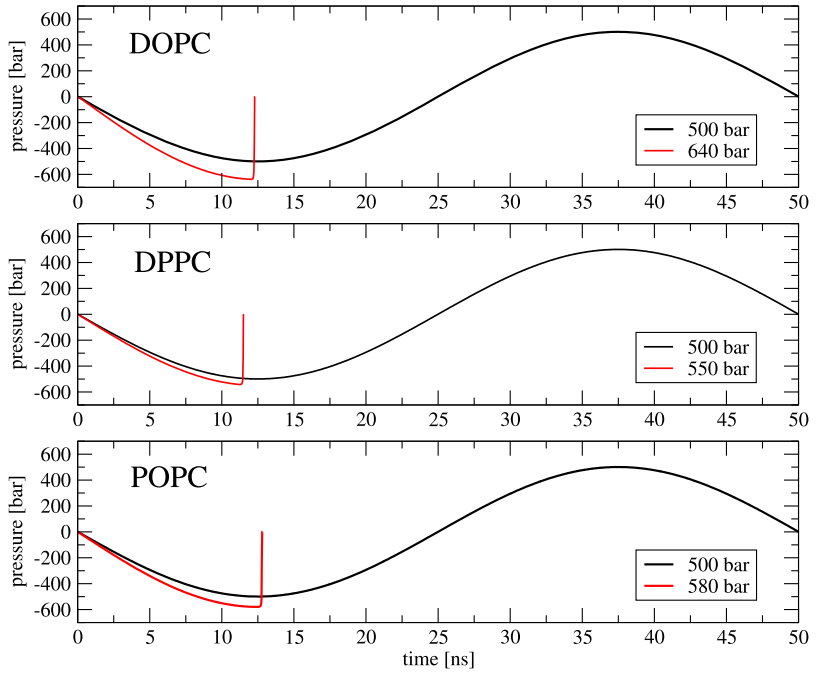

Figure 2. Time evolution of the pressure in the three liposome systems. The pressures of all systems are stably increased and decreased under an ultrasound intensity of 500 bar (black lines). At higher ultrasound intensities, the pressures drop to zero when the ultrasound amplitude is maximum around $t \sim \tau/2 = 12.5$ ns (red lines), indicating that the systems are exploded. A frequency of 20 MHz is used in all simulations. For clarity, only one ultrasound period is displayed.

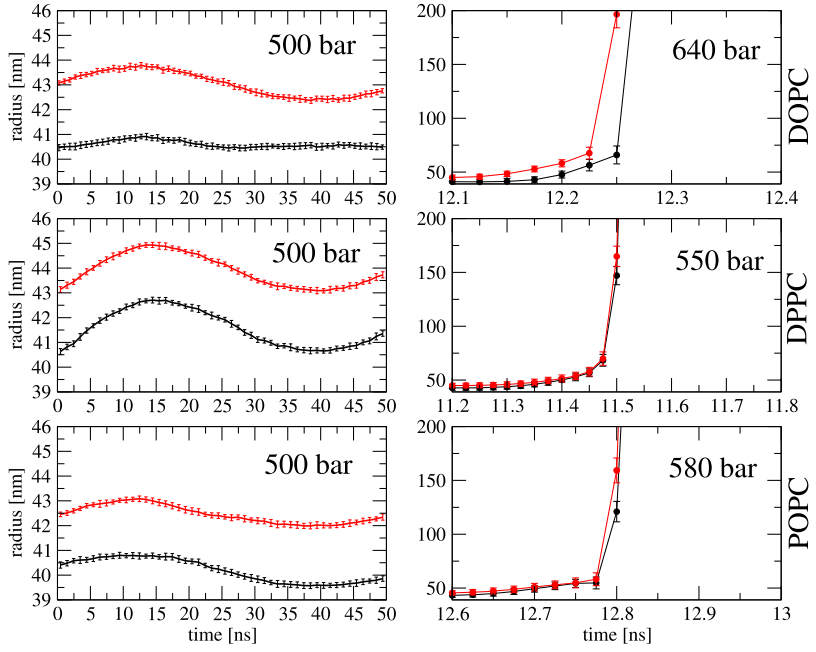

Figure 3. Time evolution of the inner (black lines) and outer (red lines) radii of the three liposomes. All liposomes are stable up to an ultrasound intensity of 500 bar (left panels) but undergo large changes at higher intensities (right panels). The error bars are estimated from five trajectories of each system. A frequency of 20 MHz is used in all simulations.

are scaled through eq 1, and the system volume becomes $\vec{V}\left[1 - \frac{\beta\Delta t}{\tau_p}(P(t) - P_0)\right]V$. This way, the instantaneous pressure $P(t)$ always fluctuates around the desired value P_0.

In an ultrasound simulation, the instantaneous pressure of the system will oscillate around the reference value P_0 following the compression and rarefaction of the sound wave. We take into account this effect of the ultrasound wave, which has the form

$$p(t) = A \sin(2\pi\omega t) \tag{3}$$

by using a modified scale factor[44]

$$\mu = \left[1 - \frac{\beta\Delta t}{\tau_p}(P(t) - P_0 - A \sin(2\pi\omega t))\right]^{1/3} \tag{4}$$

where ω and A are the frequency and amplitude of the ultrasound. The lengths of the system are then scaled as usual (eq 1). This guarantees

https://doi.org/10.1021/acs.langmuir.1c00555
Langmuir 2021, 37, 7945−7954

that the pressure of the system is always equal to the pressure of the ultrasound. In all simulations, ultrasound with frequency $\omega = 20$ MHz is used. The ultrasound amplitude is scanned from 0 to 500 bar with a step of 50 bar. Within this range, we do not observe any structural defects in liposomes. Thus, we carry simulations at a very high intensity of 700 bar, and all liposomes are destroyed immediately. Having nailed down the possible range, we then carry out simulations with ultrasound intensity in the range of 500−700 bar with an increase of 10 bar. From that, we are able to determine the intensity thresholds of 640, 580, and 550 bar for DOPC, DPPC, and POPC liposomes and 670, 630, and 650 bar for DOPC/CHL, DPPC/CHL, and POPC/CHL liposomes, respectively, at which the structural defects begin to occur. The reference pressure, $P_0 = 1$ bar, the isotropic pressure coupling constant, $\tau_p = 1$ ps, and the isothermal compressibility of 4.5×10^{-5} bar^{-1} are used. To ensure that the damage to the membrane is not due to heat generated by the work done by ultrasound, we couple both liposome and water to the heat bath at 300 K employing the Berendsen coupling method[43] with a temperature coupling constant of 0.1 ps. The equations of motion are integrated using the leapfrog algorithm with a small time step of 5 fs to ensure the stability of the simulations, instead of 20 fs as usually used in equilibrium simulations. The electrostatic interactions are calculated using the particle mesh Ewald method and a cutoff of 1.4 nm.[45] A cutoff of 1.4 nm is used for the van der Waals interactions. The nonbonded pair lists are updated every 5 fs. The data are saved for every 25 ps for subsequent analyses.

RESULTS

Ultrasound-Induced Defects in Liposomes. First, we present the results of single-component liposomes. For each system, we run five trajectories, each 200 ns long, with different ultrasound intensities. During the ultrasound rarefaction and compression phases, the system is expanded and compressed, respectively, and this induces harmonic oscillation in the system pressure, as shown in Figure 2. We find that up to the ultrasound intensity of 500 bar, all three liposomes are still very stable. We also run one long simulation for the DOPC system for 1 μs at an intensity of 500 bar, and the liposome does not show any structural defects. To find the thresholds at which pathways are formed, we increase progressively the ultrasound intensity with a step of 10 bar and find that each liposome responds differently to the ultrasound. We observe that starting from intensities A = 640, 550, and 580 bar, the pressures in the DOPC, DPPC, and POPC systems, respectively, are initially negatively increased, but around $t \sim \tau/2 = 12.5$ ns, when the ultrasound is negatively maximum, the pressures of the systems are suddenly decreased to zero, indicating that the systems undergo very large expansions (Figure 2).

To reveal the structural changes, Figure 3 shows the time evolution of the inner and outer radii of each liposome. The radius is calculated as $R(t) = \frac{1}{n}\sum_{i=1}^{n} r_i(t)$, where $r_i(t)$ is the distance between the center of the liposome and the center of mass of the i-th lipid and n is the total number of lipids pertaining to the inner or outer leaflet. Overall, at $A = 500$ bar, all three liposomes are stably expanded and compressed following the decrease and increase of the system pressures as shown in Figure 2. For the DOPC liposome, the behavior of the inner and outer radii is different: the outer radius oscillates with amplitude ∼1 nm, while the inner radius is almost constant. Both inner and outer radii of the DPPC liposome oscillate synchronously with large amplitudes of ∼2 nm. The outer radius of POPC liposome oscillates synchronously with the inner radius, but the amplitudes are relatively small. Overall, we observe that the expansion amplitude is larger than the compression amplitude. This is due to the presence of water inside the liposomes that makes the compression more difficult.

For the DOPC liposome, at A = 640 bar, the outer radius expands rapidly and ruptures at 12.22 ns, whereas the inner radius starts to expand at ∼12.17 ns and ruptures at ∼12.25 ns. This is also seen from the snapshot in Figure 1 which shows that at 12.22 ns, the outer leaflet is largely stretched, whereas the spherical topology of the inner leaflet is still maintained. This creates a large air compartment in between the two leaflets. At 12.5 ns, the outer leaflet is largely damaged; the inner leaflet, however, retained its spherical shape, though very stretched. At 550 bar, both inner and outer radii of the DPPC liposome expand and rupture at around 11.47 ns, whereas burst of both outer and inner radii of the POPC liposome is at around 580 bar and 12.77 ns. It seems that the DPPC liposome resonates more easily with ultrasound and burst at lower pressures and shorter times as compared to the DOPC and POPC liposomes. A visualization of snapshots, shown in Figure 1, reveals that the overall size of the DPPC or POPC liposome does not change much; only a pore is formed on the surface. The burst in the radii shown in Figure 3 is due to the contribution from the expelled lipids from the pore.

The above results show that the ultrasound-induced structural defect depends on the lipid composition of the liposome. For the DOPC liposome, the possible drug release pathway is through the enhanced diffusion due to the low lipid packing density induced by the stretched bilayer. In addition, the air compartment between the two leaflets also enhances the diffusive process of drugs across the membrane. We explain this based on the fact that a number of MD simulations have shown that the free-energy profile for translocation across the lipid bilayer of drugs usually exhibits a high barrier in the middle of the two leaflets.[46−49] If the two leaflets are separated apart, then the population of drugs between them is increased, that is, the free energy barrier is reduced, and therefore the drug permeability is increased. For the DPPC and DOPC liposomes, the possible drug-release pathways are through pores and/or large damaged sections on the liposome surface.

Both leaflet detachment and pore formation mechanisms can be linked to changes in lipid packing in the bilayer. For example, Mendelsohn et al. showed that ultrasound disrupts the packing of the hydrophobic lipid tails in the bilayer core.[50] Lawaczeck et al. showed that ultrasound creates structural defects in liposomes at a temperature below their phase transition.[51] Therefore, to understand the molecular origin that determines the pathway formation, we first calculate the thickness of the bilayers, and the results of the three liposomes are similar, ∼4 nm. This suggests that the bilayer thickness should not be the dominant parameter that determines the pathways as suggested by theory.[32] Next, we calculate the total potential energy between lipids pertaining to the inner or outer leaflets and the inner−outer leaflet interacting energy for each liposome in the equilibrium state; that is, without ultrasound. The results averaged over structures of last 100 ns trajectory are listed in Table 1. As seen, the inner−outer leaflet interacting energy of the DOPC liposome is $\sim 2 \times 10^5$ kJ/mol weaker than those of the DPPC and POPC liposomes, and this explains why the two leaflets of the DOPC liposome tend to be separated apart, but those of the DPPC and POPC remain close under ultrasound expansion (Figures 1, 3). In contrast, the potential energy of the individual leaflets of the DOPC liposome is $\sim 3 \times 10^5$ kJ/mol stronger than those of the DPPC and POPC counterparts, meaning that the interaction between lipids inside DOPC

https://doi.org/10.1021/acs.langmuir.1c00555
Langmuir 2021, 37, 7945−7954

Table 1. Total Potential Energy (in kJ/mol) of the Inner and Outer Leaflets and between Inner−Outer Leaflets of Six Liposomes[a]

liposome	inner leaflet	outer leaflet	inner−outer leaflets
DOPC (300 K)	−4.84 × 106	−5.34 × 106	−1.20 × 106
DPPC (300 K)	−4.57 × 106	−5.07 × 106	−1.41 × 106
POPC (300 K)	−4.59 × 106	−5.11 × 106	−1.38 × 106
DOPC/CHL (300 K)	−4.97 × 106	−5.53 × 106	−1.15 × 106
DPPC/CHL (300 K)	−4.89 × 106	−5.41 × 106	−1.30 × 106
POPC/CHL (300 K)	−4.91 × 106	−5.46 × 106	−1.25 × 106
DOPC (255 K)	−5.08 × 106	−5.60 × 106	−1.30 × 106
DPPC (314 K)	−4.54 × 106	−5.04 × 106	−1.40 × 106
POPC (270 K)	−4.96 × 106	−5.47 × 106	−1.35 × 106

[a]Shown are results obtained from the average of conformations of 100 ns equilibrium MD trajectories.

leaflets is stronger than those in the DPPC and POPC counterparts. This explains that although the two leaflets of the DOPC are separated apart, their spherical shape is largely maintained, while the interaction between lipids inside the single leaflets of the DPPC and POPC liposomes tends to be disrupted and lipids are expelled from their surfaces, forming transient or permanent pores on the surfaces (Figure 1).

Effect of CHL. Numerous studies have shown that CHL could increase the packing and stiffening of phospholipid molecules[52−54] and thus stabilize the lipid bilayer. Therefore, in drug-delivery applications, CHL is usually mixed with lipids to increase the stability of liposomes. It is of interest to understand the effect of CHL on the molecular mechanism of ultrasound-induced structural defect in liposomes. To this end, we carry out additionally three simulations for the three liposomes DOPC/CHL, DPPC/CHL, and POPC/CHL, each containing 30% CHL. This percentage is chosen because the most frequently used proportion is a 2:1 ratio (e.g., 2 parts of lipids and 1 part of CHL).[37] The same ultrasound frequency of ω = 20 MHz is used for all simulations. The results show that at the ultrasound intensity thresholds of single-component liposomes (A = 640, 550, and 580 bar for the DOPC, DPPC, and POPC liposomes, respectively), no defects are observed in the CHL mixed liposome counterparts. This is probably not surprising as CHL increases the stability of the lipid membranes.[52−54] We then increase the ultrasound intensity with a step of 10 bar, and the structural defects start to appear at intensities A = 670, 630, and 650 bar for the DOPC/CHL, DPPC/CHL, and POPC/CHL liposomes, respectively. Figure 4 shows the selected snapshots of the three liposomes during the destruction process. For the DOPC/CHL liposome, the destruction mechanism is quite similar to that of the pure DOPC liposome, where two leaflets of the membrane surface are detached (Figures 1, 4). Surprisingly, this mechanism is also observed for the DPPC/CHL and POPC/CHL liposomes, in contrast to the pore formation mechanism observed in the pure DPPC and POPC liposomes (Figure 1). To understand these results, we calculate the interleaflet and intraleaflet potential energy of these three mixed liposomes, and the results are shown in Table 1. Because CHL increases the packing and stiffening of phospholipid molecules, the intrapotential energies of both inner and outer leaflets are stronger than those of the single-component liposome counterparts. For example, the potential energy of the inner leaflet of the DOPC liposome is -4.84×10^6 kJ/mol, while it is -4.97×10^6 kJ/mol for the DOPC/CHL liposome. However, the interleaflet

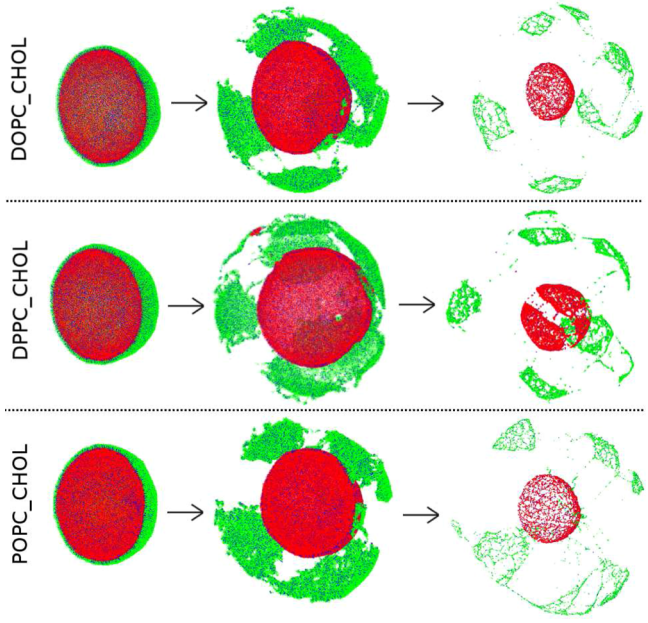

Figure 4. Selected snapshots at t = 0 ns (left), 10 ns (middle), and 12.5 ns (right) of three liposomes DOPC/CHL, DPPC/CHL, and POPC/CHL obtained from simulations using the ultrasound intensity of 670, 630, and 650 bar, respectively. The frequency of 20 MHz is used in all simulations. CHL is shown in blue color. The inner and outer leaflets are shown in red and green, respectively.

potential energy is reduced, ~10^5 kJ/mol, in all three CHL mixed liposomes. This indicates that CHL molecules help lipids inside leaflets to hold together but reduce the interaction between lipids and the two leaflets. Therefore, the two leaflets of the membrane surface tend to be separated under the expansion of ultrasound, and this explains the leaflets detachment mechanism shown in Figure 4 for CHL mixed liposomes. In all cases, the two leaflets are highly separated when the ultrasound is fully expanded at $t = \tau/4$ = 12.5 ns. Interestingly, we note that for all liposomes, when the intraleaflet energy increases, then the interleaflet energy is decreased and vice versa.

Effect of Phase Transition. Many studies have shown that the lipid membrane properties are significantly affected by the phase transition temperature T_c.[55,56] For example, the thickness, area per lipid, fluidity, and permeability of the bilayer vary greatly around T_c. The lipid membranes of the liposomes used in this work have different transition temperatures: 314 K for DPPC, 256 K for DOPC, and 271 K for POPC. However, all results presented in previous sections were obtained at a temperature of 300 K, where the DPPC liposome is in the liquid-ordered phase and DOPC and POPC are in the liquid-disordered phase. Therefore, the question is whether the molecular mechanism of ultrasound-induced structural defect in a liposome will depend on its phase? To this end, we carry out simulations for the DPPC liposome at 315 K, just above its transition temperature, and simulations at 255 and 270 K, just below T_c for DOPC and POPC, respectively. The same ultrasound frequency of ω = 20 MHz is used for all simulations. The ultrasound intensity is varied around the threshold value of each system obtained at 300 K (550, 580, and 640 bar for DPPC, POPC, and DOPC, respectively). Figure 5 shows the selected snapshots of three liposomes during the destruction process at temperatures just above or below T_c. As seen, for the DOPC liposome, the leaflet detachment mechanism is still observed in the liquid-ordered

https://doi.org/10.1021/acs.langmuir.1c00555
Langmuir 2021, 37, 7945−7954

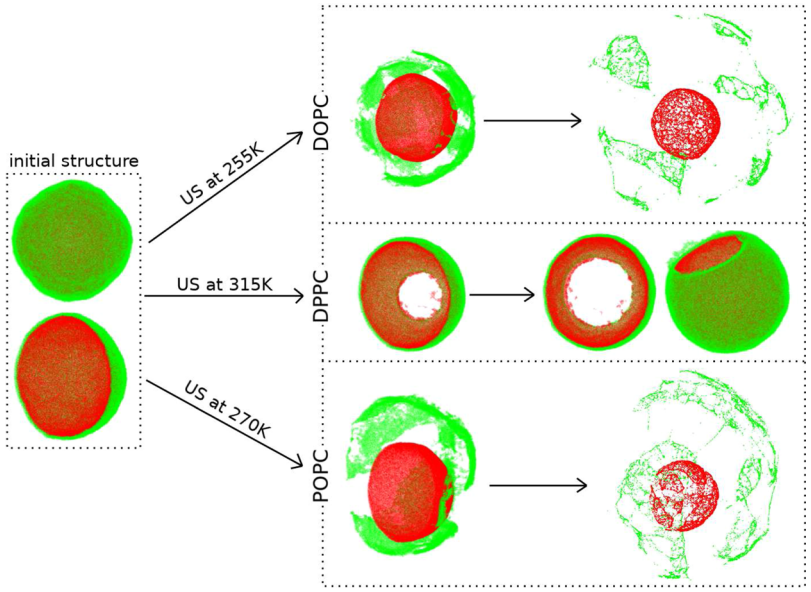

Figure 5. Initial structure (left) and snapshots of three liposomes DOPC, DPPC, and POPC obtained from simulations at temperatures just above (315 K for DPPC) or just below (255 and 270 K for DOPC and POPC, respectively) the phase transition temperatures. The ultrasound intensities of 720, 500, and 650 bar are used for the DOPC, DPPC, and POPC simulations, respectively. The frequency of 20 MHz is used in all simulations. The inner and outer leaflets are shown in red and green, respectively.

phase (T = 255 K) at 720 bar. This mechanism was already observed in the liquid-disordered phase (T = 300 K) but at a lower ultrasound intensity of 640 bar (Figure 1). For the DPPC liposome, the transient pore formation is observed in both liquid-disordered (T = 315 K, 500 bar) and liquid-ordered (T = 300 K, 550 bar) phases (Figures 1, 5). Interestingly, for the POPC liposome, the pore formation mechanism is observed in the liquid-disordered phase (T = 300 K, 580 bar, Figure 1) but switched to the leaflet detachment mechanism in the liquid-ordered phase (T = 270 K, 650 bar, Figure 5). In all cases, the ultrasound intensity required to cause the defect in a liposome in the liquid-ordered phase is higher than that in the liquid-disordered phase. We then calculate the total potential energy between lipids pertaining to the inner or outer leaflets and the inner−outer leaflet interacting energy in the equilibrium state, that is, without ultrasound, at temperatures of 255, 314, and 270 K for the DOPC, DPPC, and POPC liposome, respectively, and the results are listed in Table 1. For the DOPC liposome, on going from the liquid-disordered phase (300 K) to the liquid-ordered phase (255 K), the intraleaflet potential energies increase by ∼2.4 × 10^5 kJ/mol, while the increase of the interleaflet interaction is weaker, ∼1.2 × 10^5 kJ/mol. This means that the ultrasound that separates the two leaflets in the liquid-disordered phase (Figure 1) can also separate the two leaflets in the liquid-ordered phase (Figure 5). This explains our result that the leaflet detachment mechanism is observed in both liquid-ordered and liquid-disordered phases. For the DPPC liposome, the intraleaflet and interleaflet interactions are less affected by the transition temperature as seen by small decreases of 3 × 10^4 and 1 × 10^4 kJ/mol, respectively. This could explain that the transient pore formation mechanism seen in the liquid-ordered phase (Figure 1) is also observed in the liquid-disordered phase (Figure 5). For the POPC liposome, we observe a strong increase in the intraleaflet interaction energy, 3.7 × 10^5 kJ/mol, and a much weaker increase in the interleaflet interaction, 3 × 10^4 kJ/mol, on going from the liquid-disordered phase (300 K) to the liquid-ordered phase (270 K). The strong increase in the intraleaflet interaction prevents the escape of lipids from individual leaflets, that is, the transient pore formation mechanism is not favorable. The weak increase in the interleaflet interaction should favor the detachment of two leaflets. Therefore, the transient pore formation mechanism is switched to the leaflet detachment mechanism on going from the liquid-disordered phase (Figure 1) to the liquid-ordered phase (Figure 5) as observed.

■ DISCUSSION

To our best knowledge, there are not many experimental results on the interaction between ultrasound and liposomes, especially at the molecular level. This could be due to the fact that the release rate of drugs depends on many factors such as the molecular constituents of the lipid bilayer, temperature, type of drugs, and so forth and thus are difficult to study. Also, resolving structural defects at the molecular level is very challenging with current experimental methods. Most experiments determine the rate of ultrasound-induced release, and then mathematical models or computational modeling[27,29,31−34,57,58] are used to fit the experimental release profiles. From this, various release pathways including pore formation on the liposome surface and diffusion through the membrane or liposome destruction have been suggested. However, details of the ultrasound-induced structural defects in the membrane surface of liposomes are not well understood, especially at the molecular level.

From the theoretical side, our work presents the first ultrasound MD simulation study in the liposome field, aimed at determining the ultrasound-induced structural defects in liposomes at the molecular level. In particular, we are able to observe directly the pore formation on the liposome surface or detachment of bilayer leaflets and explain the molecular mechanism underlying these structural defects.

It is known from experiments that the timescale of drug release is on seconds. However, due to the limitation of the current computer technology, MD simulations can only capture the processes on the nanosecond−microsecond scales (200 ns

https://doi.org/10.1021/acs.langmuir.1c00555
Langmuir 2021, 37, 7945−7954

in this work). These are well-known common gaps in the time- and length-scales between experiments and simulations. In this context, our simulation study cannot be compared directly to the experimental study. However, our results still can indirectly explain some experimental findings. Indeed, Small and colleagues studied the rate of ultrasound-induced release from liposomes formed by DOPC/DPPC/CHL[25] and POPC/DPPC/CHL.[27] The bilayer permeability is obtained by fitting release kinetics to a two-film mathematical model. The results showed that DOPC/DPPC/CHL exhibits a first-order phase transition between the liquid-disordered and liquid-ordered phases, and the rate was found to be faster in the liquid-disordered phase (rich DOPC) than in the liquid-ordered phase (rich DPPC). The authors also showed that the composition of DPPC/DOPC bilayers does not affect their thickness, implying that the bilayer thickness is not responsible for the difference in rates between the two phases. However, theoretical modeling of Dan showed that the rate of release is insensitive to bilayer composition but sensitive to the bilayer thickness.[32] Our simulation shows that the response of DOPC and DPPC to ultrasound is different: two leaflets of the bilayer membrane of DOPC liposome are detached, whereas a pore is created on the lipid membrane of DPPC liposome (Figure 1). Therefore, the molecular mechanisms of ultrasound-induced drug release from DOPC and DPPC should be different, and this could explain experimental results showing that the rate was found to be different between the liquid-disordered phase (DOPC) and the liquid-ordered phase (DPPC) liposomes.[25] For the POPC/DPPC/CHL system, the experimental results showed that this system exhibits a continuous phase transition, and the rate was found to be not sensitive to the type of liquid phase but rather to the presence of domain boundaries between the two phases.[27] Our simulation results show that although POPC and DPPC have different melting temperatures, their responses to ultrasound are similar: pores are created on the surface of both the liposomes (Figure 1). Therefore, drugs should be released from these liposomes via the same pore formation mechanism, and this could explain why the release rate was experimentally found to be not sensitive to the type of liquid phase.[27]

Experimental study of Small and colleagues also showed that in general, the fraction of drug release decreases as the CHL content increases. In more detail, there are two distinct groupings of release rates, corresponding to low and high CHL fractions.[25,27] Our simulation results show that the ultrasound intensity thresholds, which induce structural defects in single-component liposomes DOPC, DPPC, and POPC, are not strong enough to induce structural defects in CHL mixed liposomes. This implies that for the same ultrasound intensity, the release rate via ultrasound-induced structural defects on the liposome surface will decrease for the CHL mixed liposomes, which are less affected by ultrasound, qualitatively in agreement with the experiment. The simulation also shows that CHL could switch the molecular mechanism from pore formation to leaflet detachment as the CHL content increases for the DPPC and POPC liposomes. Switching between two mechanisms may correspond to two groups of release rates observed by the experiment.[25,27] However, more simulations with different CHL contents should be carried out to confirm this finding. This suggests that the ratio of CHL in liposomes can be tuned to control the drug release rate. However, more simulations with different CHL contents should be carried out to confirm this finding further.

Our simulations show that the phase state of the lipid membrane of a liposome may influence the liposome-induced defect mechanism by ultrasound. It seems that for low phase transition temperature membranes such as DOPC, the leaflet detachment mechanism is probably the mechanism in both liquid-disordered and liquid-ordered phases. In contrast, the transient pore formation mechanism is the mechanism in both phases of high phase transition temperature membranes such as DPPC. For the POPC, the mechanism can be switched from leaflet detachment to transient pore formation on going from the liquid-ordered to liquid-disordered phase. However, more simulations need to be performed with lipid membranes with different phase transition temperatures to confirm our finding. Nevertheless, in all cases, the ultrasound intensity thresholds that induce defects in the liposomes in the liquid-ordered phase are higher than those in the liquid-disordered phase. This is understandable because a low temperature below the phase transition could increase the packing and stiffening of phospholipid molecules. Indeed, Kudo and colleagues carried out experiments for five liposomes with different transition temperatures between liquid-crystalline and gel phases in the range from −22 to +55 °C and showed that liposomes with lipid membranes in the gel phase have higher stability under exposure to ultrasound.[59]

The present study has some limitations of which we are fully aware. First, our simulation results could support some experimental findings, but because we do not simulate drug molecules explicitly, we cannot obtain any release rates to compare directly with experiments. Nevertheless, the simulation could provide detailed information on the pore size and distribution, the diffusion constant through the stretched surface, and the formation of the air compartments inside the bilayer. This information may complement experimental and mathematical modeling results. Second, to be close to experiments, the diameter of our liposomes, ∼80 nm, is similar to that of experimental liposomes (∼100 nm). To our best knowledge, this is the first MD simulation study of such big liposomes. However, current computer technology only allows simulation durations to be in the nanosecond timescale, which is much shorter than the second timescale in experiments. Thus, we have to use high intensity and fast frequency ultrasound in order to observe reasonable ultrasound effects on reasonable timescales. However, since the formation of pathways is essentially determined by the molecular interaction between lipids as shown above, we expect that the pathways seen in the simulation would also be the pathways obtained in the experiment. However, we note that the rate of release may vary between simulation and experiment because the timescales of simulations and experiments are different, and proving this is beyond the scope of this paper. Third, to verify whether the release pathways depend on the use of coarse-grained MARTINI force field, we carry out a simulation using the all-atom CHARMM36 force field[41] for a DOPC liposome. An all-atom system of liposome with a diameter of 80 nm contains ∼54 × 10^6 atoms, including waters which is too large for the simulation. Therefore, to be feasible, we consider a smaller all-atom liposome with a diameter of 20 nm. We use the same ultrasound intensity A = 640 bar and frequency ω = 20 MHz as that used for the coarse-grained counterpart. Interestingly, the snapshots shown in Figure 1 indicate that the responses of the all-atom and coarse-grained liposomes are quite similar: two leaflets are detached, and each leaflet is stretched due to the ultrasound expansion. This suggests that the ultrasound-induced

https://doi.org/10.1021/acs.langmuir.1c00555
Langmuir 2021, 37, 7945−7954

pathways are insensitive to the force fields and also to the size of the liposome. Indeed, we should mention that the coarse-grained MARTINI force field has been used in several nonequilibrium MD simulations to study the interaction between bubble collapse and shockwave with lipid membranes,[60−70] stress propagation in lipid bilayers,[71] and pore formation by external electric field.[72] Overall, the results are in good agreement with experiments or atomistic simulation results. This gives us confidence, and we believe that the essential pathways induced by ultrasound on liposomes shown above are insensitive to the force fields.

CONCLUSIONS

We have carried out for the first time large-scale MD simulations of single lipid component liposomes as well as CHL mixed liposomes under ultrasound to identify defects on the liposome surface where drugs can be released from the liposome. We observe two types of defects: pore formation on the liposome surface or detachment of bilayer leaflets, depending on the lipid composition and CHL content. We show that the molecular origin that determines the formation of defects is the competition between the intraleaflet and interleaflet interactions of lipids. If the intraleaflet energy is dominant, then the leaflet detachment is the main mechanism. In contrast, if the interleaflet energy is dominant, then the pore formation is the main mechanism. CHL could increase the packing and stiffening of phospholipid molecules, and thus it can switch the pore formation mechanism to the leaflet detachment mechanism. We show that the phase state of the lipid membrane also influences the mechanism. For the low phase transition temperature DOPC liposome, the detachment between the bilayer membrane is the mechanism in both liquid-ordered and liquid-disordered phases. In contrast, for the high phase transition temperature DPPC liposome, the formation of the transient pore is the mechanism in both liquid-disordered and liquid-ordered phases. For the POPC liposome, the detachment between the bilayer membrane mechanism is observed in the liquid-ordered phase, but the transient pore formation is the mechanism in the liquid-disordered phase. Our simulation results can support and interpret some experimental and mathematical modeling studies. In general, the simulation can complement experiments and mathematical modeling to identify exactly the pathway-rate relationship and interpret the mechanism at the molecular level. This could help manufacturers asses the specific role of each pathway to design efficient drug-delivery systems that meet user requirements. However, to assess the rates, drugs must be considered explicitly in the simulation, and this work is underway.

AUTHOR INFORMATION

Corresponding Author

Phuong H. Nguyen − *CNRS, Université de Paris, UPR9080, Laboratoire de Biochimie Théorique, Paris, France, Institut de Biologie Physico-Chimique, Fondation Edmond de Rothschild, PSL Research University, Paris 75005, France;* orcid.org/0000-0003-1284-967X; Email: nguyen@ibpc.fr

Authors

Viet Hoang Man − *Department of Pharmaceutical Sciences, School of Pharmacy, University of Pittsburgh, Pittsburgh, Pennsylvania 15213, United States;* orcid.org/0000-0002-8907-6479

Mai Suan Li − *Institute of Physics, Polish Academy of Sciences, 02-668 Warsaw, Poland; Institute for Computational Science and Technology, Ho Chi Minh City, Vietnam;* orcid.org/0000-0001-7021-7916

Philippe Derreumaux − *CNRS, Université de Paris, UPR9080, Laboratoire de Biochimie Théorique, Paris, France, Institut de Biologie Physico-Chimique, Fondation Edmond de Rothschild, PSL Research University, Paris 75005, France;* orcid.org/0000-0001-9110-5585

Junmei Wang − *Department of Pharmaceutical Sciences, School of Pharmacy, University of Pittsburgh, Pittsburgh, Pennsylvania 15213, United States;* orcid.org/0000-0002-9607-8229

Complete contact information is available at: https://pubs.acs.org/10.1021/acs.langmuir.1c00555

Author Contributions

V.H.M. and M.S.L. contributed equally to this work.

Notes

The authors declare no competing financial interest.

ACKNOWLEDGMENTS

This work has been supported by the Department of Science and Technology at Ho Chi Minh City, Vietnam (grant 13/2020/HD-QPTKHCN), CNRS, the National Science Foundation (NSF, grant SI2-SEE-1534941), the National Institutes of Health (NIH-R01GM118508), and the CINES/TGCC/IDRIS centers for providing computer facilities (projects A0080711440, A0090711988).

REFERENCES

(1) Kohane, D. S. Microparticles and nanoparticles for drug delivery. *Biotechnol. Bioeng.* **2007**, *96*, 203−209.

(2) Wang, F.; Shi, Y.; Lu, L.; Liu, L.; Cai, Y.; Zheng, H.; Liu, X.; Yan, F.; Zou, C.; Sun, C.; et al. Targeted delivery of GDNF through the blood-brain barrier by MRI-guided focused ultrasound. *PLoS One* **2012**, *7*, No. e52925.

(3) Chen, J.; Jiang, H.; Wu, Y.; Li, Y.; Gao, Y. A novel glycyrrhetinic acid-modified oxaliplatin liposome for liver-targeting and in vitro/vivo evaluation. *Drug Des., Dev. Ther.* **2015**, *9*, 2265−2275.

(4) Parveen, S.; Misra, R.; Sahoo, S. K. Nanoparticles: a boon to drug delivery, therapeutics, diagnostics and imaging. *Nanomedicine* **2012**, *8*, 147−166.

(5) Martinelli, C.; Pucci, C.; Ciofani, G. Nanostructured carriers as innovative tools for cancer diagnosis and therapy. *APL Bioeng.* **2019**, *3*, 011502.

(6) Blanco, E.; Shen, H.; Ferrari, M. Principles of nanoparticle design for overcoming biological barriers to drug delivery. *Nat. Biotechnol.* **2015**, *33*, 941−951.

(7) Obata, Y.; Tajima, S.; Takeoka, S. Evaluation of pH-responsive liposomes containing amino acid-based zwitterionic lipids for improving intracellular drug delivery in vitro and in vivo. *J. Controlled Release* **2010**, *142*, 267.

(8) Tannock, I. F.; Rotin, D. Acid pH in tumors and its potential for therapeutic exploitation. *Cancer Res.* **1989**, *49*, 4373.

(9) Wang, Y.-C.; Wang, F.; Sun, T.-M.; Wang, J. Redox-responsive nanoparticles from the single disulfide bond-bridged block copolymer as drug carriers for overcoming multidrug resistance in cancer cells. *Bioconjugate Chem.* **2011**, *22*, 1939.

(10) Needham, D.; Anyarambhatla, G.; Kong, G.; Dewhirst, M. W. A new temperature-sensitive liposome for use with mild hyperthermia: Characterization and testing in a human tumor xenograft model. *Cancer Res.* **2000**, *60*, 1197.

(11) Dicheva, B. M.; Koning, G. A. Targeted thermosensitive liposomes: An attractive novel approach for increased drug delivery to solid tumors. *Expert Opin. Drug Delivery* **2014**, *11*, 83.
(12) Fomina, N.; McFearin, C.; Sermsakdi, M.; Edigin, O.; Almutairi, A. UV and near-IR triggered release from polymeric nanoparticles. *J. Am. Chem. Soc.* **2010**, *132*, 9540.
(13) Schroeder, A.; Honen, R.; Turjeman, K.; Gabizon, A.; Kost, J.; Barenholz, Y. Ultrasound triggered release of cisplatin from liposomes in murine tumors. *J. Controlled Release* **2009**, *137*, 63.
(14) Benival, D. M.; Devarajan, P. V. Lipomer of doxorubicin hydrochloride for enhanced oral bioavailability. *Int. J. Pharm.* **2012**, *423*, 554−561.
(15) Alibolandi, M.; Abnous, K.; Sadeghi, F.; Hosseinkhani, H.; Ramezani, M.; Hadizadeh, F. Folate receptor-targeted multimodal polymersomes for delivery of quantum dots and doxorubicin to breast adenocarcinoma: in vitro and in vivo evaluation. *Int. J. Pharm.* **2016**, *500*, 162−178.
(16) Olson, J. A.; Schwartz, J. A.; Hahka, D.; Nguyen, N.; Bunch, T.; Jensen, G. M.; Adler-Moore, J. P. Toxicity and efficacy differences between liposomal amphotericin B formulations in uninfected and Aspergillus fumigatus infected mice. *Med. Mycol. J.* **2015**, *53*, 107−118.
(17) D'Mello, S. R.; Cruz, C. N.; Chen, M.; Kapoor, M.; Lee, S. L.; Tyner, K. M. The evolving landscape of drug products containing nanomaterials in the United States. *Nat. Nanotechnol.* **2017**, *12*, 523−529.
(18) Frenkel, V. Ultrasound mediated delivery of drugs and genes to solid tumors. *Adv. Drug Deliv. Rev.* **2008**, *60*, 1193−1208.
(19) Pitt, W. G.; Husseini, G. A.; Staples, B. J. Ultrasonic drug delivery - a general review. *Expert Opin. Drug Delivery* **2004**, *1*, 37−56.
(20) Dromi, S.; Frenkel, V.; Luk, A.; Traughber, B.; Angstadt, M.; Bur, M.; Poff, J.; Xie, J.; Libutti, S. K.; Li, K. C. P.; et al. Pulsed-High Intensity Focused Ultrasound and Low Temperature-Sensitive Liposomes for Enhanced Targeted Drug Delivery and Antitumor Effect. *Clin. Cancer Res.* **2007**, *13*, 2722−2727.
(21) Rapoport, S. I. Advances in osmotic opening of the blood-brain barrier to enhance CNS chemotherapy. *Expert Opin. Invest. Drugs* **2001**, *10*, 1809.
(22) Gao, Z.-G.; Fain, H. D.; Rapoport, N. Controlled and targeted tumor chemotherapy by micellar-encapsulated drug and ultrasound. *J. Controlled Release* **2005**, *102*, 203.
(23) Schroeder, A.; Avnir, Y.; Weisman, S.; Najajreh, Y.; Gabizon, A.; Talmon, Y.; Kost, J.; Barenholz, Y. Controlling liposomal drug release with low frequency ultrasound: mechanism and feasibility. *Langmuir* **2007**, *23*, 4019−4025.
(24) Schroeder, A.; Kost, J.; Barenholz, Y. Ultrasound, Liposomes, and Drug Delivery: Principles for Using Ultrasound to Control the Release of Drugs From Liposomes. *Phys. Chem. Liq.* **2009**, *162*, 1−16.
(25) Small, E. F.; Willy, M. C.; Lewin, P. A.; Wrenn, S. P. Ultrasound-induced transport across lipid bilayers: influence of phase behavior. *Colloids Surf., A* **2011**, *390*, 40−47.
(26) Wrenn, S. P.; Dicker, S. M.; Small, E. F.; Dan, N. R.; Mleczko, M.; Schmitz, G.; Lewin, P. A. Bursting Bubbles and Bilayers. *Theranostics* **2012**, *2*, 1140.
(27) Small, E. F.; Dan, N. R.; Wrenn, S. P. Low-frequency ultrasound-induced transport across non-raft-forming ternary lipid bilayers. *Langmuir* **2012**, *28*, 14364−14372.
(28) Evjen, T. J.; Hupfeld, S.; Barnert, S.; Fossheim, S.; Schubert, R.; Brandl, M. Physicochemical characterization of liposomes after ultrasound exposure - mechanisms of drug release. *J. Pharm. Biomed. Anal.* **2013**, *78*−*79*, 118−122.
(29) Enden, G.; Schroeder, A. A mathematical Model of Drug Release from Liposomes by Low Frequency Ultrasound. *Ann. Biomed. Eng.* **2009**, *37*, 2640−2645.
(30) Simon, L.; Ospina, J. On the effusion time of drugs from the open pore of a spherical vesicle. *Physica A* **2016**, *451*, 366−372.
(31) Siepmann, J.; Siepmann, F. Mathematical modeling of drug delivery. *Int. J. Pharm.* **2008**, *364*, 328−343.
(32) Wrenn, S. P.; Small, E.; Dan, N. Bubble nucleation in lipid bilayers: a mechanism for low frequency ultrasound disruption. *Biochim. Biophys. Acta* **2013**, *1828*, 1192−1197.
(33) Dan, N. Nanostructured lipid carriers: effect of solid phase fraction and distribution on the release of encapsulated materials. *Langmuir* **2014**, *30*, 13809−13814.
(34) Dan, N. Drug release through liposome pores. *Colloids Surf., B* **2015**, *126*, 80−86.
(35) Nele, V.; Holme, M. N.; Kauscher, U.; Thomas, M. R.; Doutch, J. J.; Stevens, M. M. Effect of Formulation Method, Lipid Composition, and PEGylation on Vesicle Lamellarity: A Small-Angle Neutron Scattering Study. *Langmuir* **2019**, *35*, 6064−6074.
(36) Margalit, R.; Alon, R.; Linenberg, M.; Rubin, I.; Roseman, T. J.; Wood, R. W. Liposomal drug delivery: thermodynamic and chemical kinetic considerations. *J. Controlled Release* **1991**, *17*, 285−296.
(37) Briuglia, M.-L.; Rotella, C.; McFarlane, A.; Lamprou, D. A. Influence of cholesterol on liposome stability and on in vitro drug release. *Drug Delivery Transl. Res.* **2015**, *5*, 231−242.
(38) Wang, Y.; Gkeka, P.; Fuchs, J. E.; Liedl, K. R.; Cournia, Z. DPPC-cholesterol phase diagram using coarse-grained Molecular Dynamics simulations. *Biochim. Biophys. Acta, Biomembr.* **2016**, *1858*, 2846−2857.
(39) Marrink, S. J.; Risselada, H. J.; Yefimov, S.; Tieleman, D. P.; de Vries, A. H. The MARTINI Force Field: Coarse Grained Model for Biomolecular Simulations. *J. Phys. Chem. B* **2007**, *111*, 7812−7824.
(40) Marrink, S. J.; Tieleman, D. P. Perspective on the Martini model. *Chem. Soc. Rev.* **2013**, *42*, 6801−6822.
(41) MacKerell, A. D., Jr; Bashford, D.; Bellott, M.; Dunbrack, R. L.; Evanseck, J. D.; Field, M. J.; Fischer, S.; Gao, J.; Guo, H.; Ha, S.; et al. All-atom empirical potential for molecular modeling and dynamics studies of proteins. *J. Phys. Chem. B* **1998**, *102*, 3586−3616.
(42) Lindahl, E.; Hess, B.; van der Spoel, D. GROMACS 3.0: A Package for Molecular Simulation and Trajectory Analysis. *J. Mol. Model.* **2001**, *7*, 306−317.
(43) Berendsen, H. J. C.; Postma, J. P. M.; van Gunsteren, W. F.; Dinola, A.; Haak, J. R. Molecular dynamics with coupling to an external bath. *J. Chem. Phys.* **1984**, *81*, 3684−3690.
(44) Man, V. H.; Li, M. S.; Derreumaux, P.; Wang, J.; Nguyen, T. T.; Nangia, S.; Nguyen, P. H. Molecular mechanism of ultrasound interaction with a blood brain barrier model. *J. Chem. Phys.* **2020**, *153*, 045104.
(45) Darden, T.; York, D.; Pedersen, L. Particle mesh Ewald: AnN·log(N) method for Ewald sums in large systems. *J. Chem. Phys.* **1993**, *98*, 10089−10092.
(46) Shinoda, W. Permeability across lipid membranes. *Biochim. Biophys. Acta, Biomembr.* **2016**, *1858*, 2254−2265.
(47) Orsi, M.; Sanderson, W. E.; Essex, J. W. Permeability of Small Molecules through a Lipid Bilayer: A Multiscale Simulation Study. *J. Phys. Chem. B* **2009**, *113*, 12019−12029.
(48) Xiang, T.-x.; Anderson, B. D. Molecular dissolution processes in lipid bilayers: A molecular dynamics simulation. *J. Chem. Phys.* **1999**, *110*, 1807−1818.
(49) Wang, Y.; Cohen, J.; Boron, W. F.; Schulten, K.; Tajkhorshid, E. Exploring gas permeability of cellular membranes and membrane channels with molecular dynamics. *J. Struct. Biol.* **2007**, *157*, 534−544.
(50) Mendelsohn, R.; Sunder, S.; Bernstein, H. J. The effect of sonication on the hydrocarbon chain conformation in model membrane systems: A Raman spectroscopic study. *Biochim. Biophys. Acta* **1976**, *419*, 563−569.
(51) Lawaczeck, R.; Kainosho, M.; Chan, S. I. The formation and annealing of structural defects in lipid bilayer vesicles. *Biochim. Biophys. Acta* **1976**, *443*, 313−330.
(52) Filippov, A.; Orädd, G.; Lindblom, G. The Effect of Cholesterol on the Lateral Diffusion of Phospholipids in Oriented Bilayers. *Biophys. J.* **2003**, *84*, 3079−3086.
(53) Ferreira, T. M.; Coreta-Gomes, F.; Ollila, O. H. S.; Moreno, M. J.; Vaz, W. L. C.; Topgaard, D. Cholesterol and POPC segmental order parameters in lipid membranes: solid state1H-13C NMR and MD simulation studies. *Phys. Chem. Chem. Phys.* **2013**, *15*, 1976−1989.

https://doi.org/10.1021/acs.langmuir.1c00555
Langmuir 2021, 37, 7945−7954

(54) Chakraborty, S.; Doktorova, M.; Molugu, T. R.; Heberle, F. A.; Scott, H. L.; Dzikovski, B.; Nagao, M.; Stingaciu, L.-R.; Standaert, R. F.; Barrera, F. N.; et al. How cholesterol stiffens unsaturated lipid membranes. *Proc. Natl. Acad. Sci. U.S.A.* **2020**, *117*, 21896−21905.
(55) Chapman, D. Phase transitions and fluidity characteristics of lipids and cell membranes. *Q. Rev. Biophys.* **1975**, *8*, 185.
(56) Nagle, J. F. Theory of the Main Lipid Bilayer Phase Transition. *Annu. Rev. Phys. Chem.* **1980**, *31*, 157.
(57) Higuchi, T. Mechanism of sustained-action medication. Theoretical analysis of rate of release of solid drugs dispersed in solid matrices. *J. Pharm. Sci.* **1963**, *52*, 1145−1149.
(58) Mircioiu, C.; Voicu, V.; Anuta, V.; Tudose, A.; Celia, C.; Paolino, D.; Fresta, M.; Sandulovici, R.; Mircioiu, I. Mathematical Modeling of Release Kinetics from Supramolecular Drug Delivery Systems. *Pharmaceutics* **2019**, *11*, 140.
(59) Kudo, N.; Sakaguchi, K.; Suzuki, R.; Maruyama, K. Effects of Phase Transition of a Lipid Bilayer on Dynamics of Bubble Liposomes. *2009 IEEE International Ultrasonics Symposium*; IEEE, 2009; p 1255.
(60) Ganzenmüller, G. C.; Hiermaier, S.; Steinhauser, M. O. Shock-wave induced damage in lipid bilayers: a dissipative particle dynamics simulation study. *Soft Matter* **2011**, *7*, 4307−4317.
(61) Choubey, A.; Vedadi, M.; Nomura, K.-i.; Kalia, R. K.; Nakano, A.; Vashishta, P. Poration of Lipid Bilayers by Shock-Induced Nanobubble Collapse. *Appl. Phys. Lett.* **2011**, *98*, 023701.
(62) Schanz, D.; Metten, B.; Kurz, T.; Lauterborn, W. Molecular Dynamics Simulations of Cavitation Bubble Collapse and Sonoluminescence. *New J. Phys.* **2012**, *14*, 113019.
(63) Shekhar, A.; Nomura, K.; Kalia, R. K.; Nakano, A.; Vashishta, P. Nanobubble Collapse on a Silica Surface in Water: Billion-Atom Reactive Molecular Dynamics Simulations. *Phys. Rev. Lett.* **2013**, *111*, 184503.
(64) Santo, K. P.; Berkowitz, M. L. Shock Wave Induced Collapse of Arrays of Nanobubbles Located Next to a Lipid Membrane: Coarse-Grained Computer Simulations. *J. Phys. Chem. B* **2014**, *119*, 8879−8889.
(65) Santo, K. P.; Berkowitz, M. L. Shock Wave Interaction with a Phospholipid Membrane: Coarse-Grained Computer Simulations. *J. Chem. Phys.* **2014**, *140*, 054906.
(66) Adhikari, U.; Goliaei, A.; Berkowitz, M. L. Mechanism of Membrane Poration by Shock Wave Induced Nanobubble Collapse: A Molecular Dynamics Study. *J. Phys. Chem. B* **2015**, *119*, 6225.
(67) Fu, H.; Comer, J.; Cai, W.; Chipot, C. Sonoporation at Small and Large Length Scales: Effect of Cavitation Bubble Collapse on Membranes. *J. Phys. Chem. Lett.* **2015**, *6*, 413−418.
(68) Koshiyama, K.; Wada, S. Collapse of a Lipid-Coated Nanobubble and Subsequent Liposome Formation. *Sci. Rep.* **2016**, *6*, 28164.
(69) Min, S. H.; Berkowitz, M. L. A comparative computational study of coarse-grained and all-atom water models in shock Hugoniot states. *J. Chem. Phys.* **2018**, *148*, 144504.
(70) Man, V. H.; Truong, P.M.; Li, M. S.; Wang, J.; Van-Oanh, N.-T.; Derreumaux, P.; Nguyen, P. H. Molecular mechanism of the cell membrane pore formation induced by bubble stable cavitation. *J. Phys. Chem. B* **2019**, *123*, 71.
(71) Aponte-Santamaría, C.; Brunken, J.; Gräter, F. Stress Propagation through Biological Lipid Bilayers in Silico. *J. Am. Chem. Soc.* **2017**, *139*, 13588.
(72) Kirsch, S. A.; Böckmann, R. A. Membrane pore formation in atomistic and coarse-grained simulations. *Biochim. Biophys. Acta* **2016**, *1858*, 2266.

https://doi.org/10.1021/acs.langmuir.1c00555
Langmuir 2021, 37, 7945−7954